High-field fMRI unveils orientation columns in humans

Essa Yacoub*, Noam Harel*†, and Kâmil Uğurbil*‡

*Center for Magnetic Resonance Research, Department of Radiology, University of Minnesota Medical School, 2021 6th Street SE, Minneapolis, MN 55455; and ‡Hochfeld Magnetresonanz Zentrum, Max Planck Institute for Biological Cybernetics, Spemannstrasse 41, Tübingen 72076, Germany

Communicated by Robert G. Shulman, Yale University, New Haven, CT, May 1, 2008 (received for review November 28, 2007)

Functional (f)MRI has revolutionized the field of human brain research. fMRI can noninvasively map the spatial architecture of brain function via localized increases in blood flow after sensory or cognitive stimulation. Recent advances in fMRI have led to enhanced sensitivity and spatial accuracy of the measured signals, indicating the possibility of detecting small neuronal ensembles that constitute fundamental computational units in the brain, such as cortical columns. Orientation columns in visual cortex are perhaps the best known example of such a functional organization in the brain. They cannot be discerned via anatomical characteristics, as with ocular dominance columns. Instead, the elucidation of their organization requires functional imaging methods. However, because of insufficient sensitivity, spatial accuracy, and image resolution of the available mapping techniques, thus far, they have not been detected in humans. Here, we demonstrate, by using high-field (7-T) fMRI, the existence and spatial features of orientation-selective columns in humans. Striking similarities were found with the known spatial features of these columns in monkeys. In addition, we found that a larger number of orientation columns are devoted to processing orientations around 90° (vertical stimuli with horizontal motion), whereas relatively similar fMRI signal changes were observed across any given active column. With the current proliferation of high-field MRI systems and constant evolution of fMRI techniques, this study heralds the exciting prospect of exploring unmapped and/or unknown columnar level functional organizations in the human brain.

blood oxygen level-dependent contrast | cortical map | high resolution | spin echo | 7-tesla

High-field MRI has pushed the level of detail to which submillimeter functional organizations can be mapped with fMRI because of increases in the signal-to-noise ratio (1) and the spatial accuracy of the functional signals (2). These gains are of critical importance because in the mammalian cortex, small functional cortical units that are repeated several times throughout a cortical area appear to constitute fundamental units of computation (3) that underlie mechanisms operative in brain function. One example of these fundamental units is cortical columns, a cluster of neurons with similar functional preferences spanning from the pial surface to the white matter. To no surprise, since their discovery in the somatosensory cortex (4), cortical columns have been identified across the cortex (5) and investigated in great detail (4, 6–8). In the visual cortex, preference to the right or left eye (ocular dominance), direction of motion, spatial frequency, and orientation have all been characterized (9–15). In humans, the first and, to date, the only example of such functional domains ever to have been identified is ocular dominance columns (ODCs). These were first observed by using anatomical staining techniques in the postmortem human brain of subjects who had lost sight in one eye (16). They were found to be ≈1 mm in width organized in a periodic layout in primary visual cortex. However, the unique anatomical connectivity that render ODCs visible with staining techniques does not exist for other columnar ensembles, such as orientation domains, because there is no obvious clinical symptom that would reveal their presence. Thus, in general, the ability to probe the existence of columnar systems in the human requires a highly sensitive noninvasive *in vivo* technique.

To date, several studies using fMRI have succeeded in mapping ODCs in humans (17–21). However, since the initial ODC fMRI work in humans, there have been no additional studies or developments in this pursuit until recently (21, 22). This prolonged silence is a reflection of the difficulty and limitations of the early approaches as general methods for exploring previously unmapped columnar organizations in the human brain. Our recent study of human ODCs (21) represents a culmination of a series of theoretical and experimental studies on mechanisms of fMRI contrast, with particular focus on the effects of magnetic field strength and image contrast preparation, and extensive verifications by using animal models (e.g., refs. 2 and 23–25). In the human ODC work (21), we demonstrated that BOLD (blood oxygen level-dependent) contrast sampled not with conventional gradient echo (GE) but probed through spin echoes (SE) at ultrahigh magnetic fields (7 T), yielded accurate and reproducible (over days) ODC maps that were unaffected by nonspecific large vessels, which normally degrade the accuracy of GE-BOLD maps. In addition, we demonstrated that although the overall stimulus invoked changes in fMRI signal intensity were larger for GE-BOLD, column-specific differential mapping signals had a larger contrast-to-noise ratio (CNR) for SE-BOLD at 7 T. This work indicated that high-field SE-BOLD provides a more generalized high-resolution mapping methodology that could be used to explore unmapped columnar systems in the human brain. As such, we have used a similar approach to investigate the organization for orientation preference in primary visual cortex, a columnar architecture that has been shown to exist in animal models (e.g., refs. 10, 11, 13, 23, and 25–27 and references therein) but has never been mapped in the human. Recent studies (28, 29) have demonstrated the presence of voxels with orientation preferences in humans by using fMRI; however, these low-resolution studies lack any information regarding the intrinsic spatial organization of these preferences. In this study, we report the existence and spatial features of orientation preference in the human brain at the columnar level and determine their spatial relationship to ODCs. The results illustrate that the high-field spin echo BOLD fMRI approach provides the means to investigate unknown submillimeter functional architectures in humans, potentially paving the way for future explorations of such fundamental computational units.

Results and Discussion

ODC and orientation preference maps, two well explored functional organizations, are known to coexist and overlap across cortical tissue in primary visual cortex (V1). Animal model studies have described several general features in the spatial organization of each map and their interdependence (30–32). These features serve as a test for the veracity of the maps obtained in the human brain in the present study.

Author contributions: E.Y., N.H., and K.U. designed research; E.Y. and N.H. performed research; E.Y. and N.H. analyzed data; and E.Y., N.H., and K.U. wrote the paper.

The authors declare no conflict of interest.

†To whom correspondence should be addressed. E-mail: noam@cmrr.umn.edu

This article contains supporting information online at www.pnas.org/cgi/content/full/0804110105/DCSupplemental.

NEUROSCIENCE

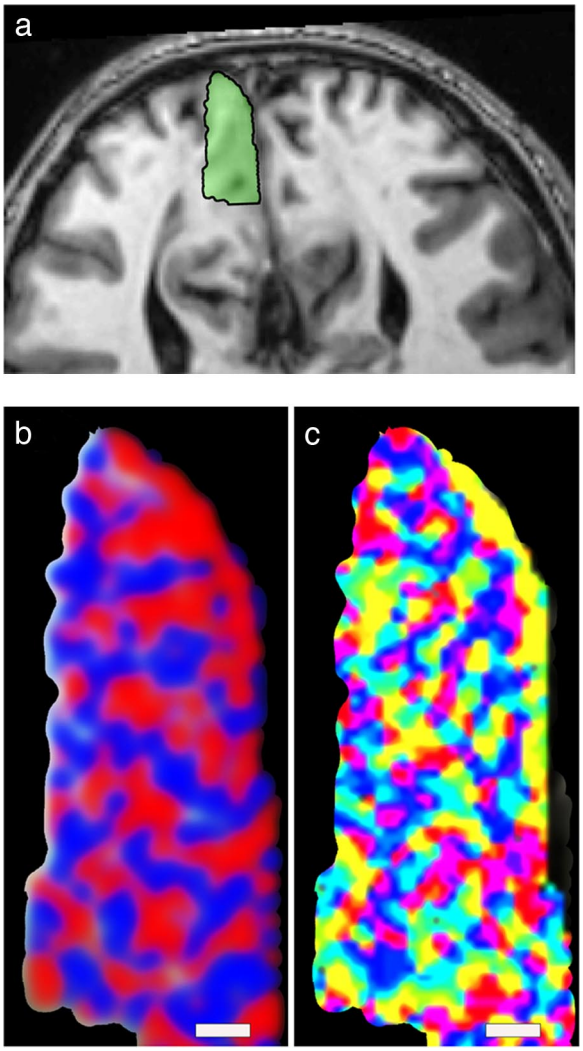

Fig. 1. Slice selection and functional domains in human visual cortex. *a* depicts the optimal region of flat gray matter in primary visual cortex (parallel to the calcarine sulcus) in one subject from which columnar level fMRI maps of ODC (*b*) and orientation preference (*c*) are generated and characterized. The functional maps in *b* and *c* are zoomed views of the ROI in *a*. The red and blue colors in *b* indicate preferences to right or left eye stimulation, whereas the color distribution in *c* represents a given voxel's fMRI time course phase, which is indicative of its preferred stimulus orientation. (Scale bar: 1.0 mm.)

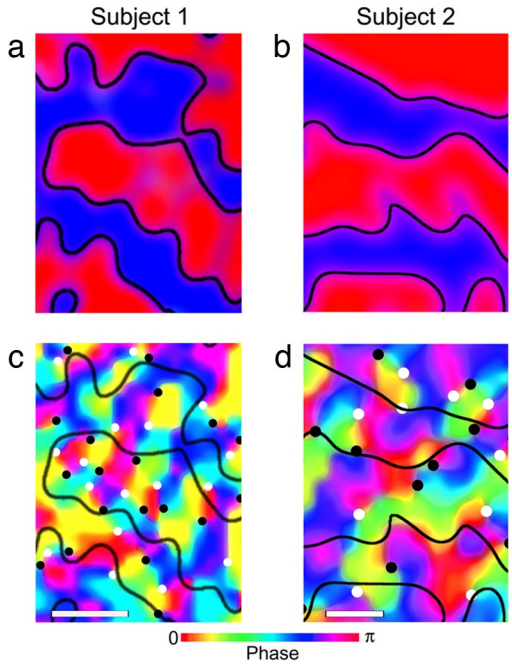

Fig. 2. Ocular dominance and orientation columns in human visual cortex. Shown in *a* and *b* are additionally zoomed ODC maps from the image in Fig. 1*b* (subject 1) and from another subject (subject 2), respectively. Red and blue represent voxels that demonstrated preference to right and left eye stimulation, respectively. fMRI maps in *c* and *d* depict the orientation preference maps from the same cortical areas as their corresponding ODC maps in *a* and *b*, respectively. ODC borders are marked with solid black lines on both the ODC and orientation maps. The black and white circles on the orientation preference maps represent areas where multiple preferences converge, or the so called pinwheel centers. This radial arrangement can be either CW (white) or CCW (black). (Color bar: calculated phase at the stimulus frequency; scale bar: 0.5 mm.)

Functional maps of ODCs and orientation preference are best visualized on a flat gray matter region of V1, in an area with minimal curvature. Such flat regions permit the use of optical imaging in animal models and single-slice fMRI for animal or human studies. Here, the human studies were conducted by using a single slice in selected individuals with a flat region located in a subsection of V1. Even though fMRI maps were generated over a larger region, only expanded views from this flat region are presented (see Fig. 1).

Subjects initially participated in studies designed to resolve ODCs (21). Similar to the ODC maps in the monkey (26, 33, 34) and previous human anatomical (16, 35) and functional (19, 21) studies, preferences to right vs. left eye stimulation were observed as parallel bands modulating in 2-mm cycles (21). We have also demonstrated that such ODC maps are reproducible over days (21). This allowed us to map the ODCs in a separate session and subsequently bring the subjects back to map orientation preference by using a temporal phase-encoding paradigm with the same slice prescription. Thus, the two columnar systems, ODC and orientation preference, were mapped onto the same cortical region in the same subject. Fig. 1*a* illustrates, for subject 1, the anatomical region that was sampled across the flat cortex in V1 ([which was determined by standard retinotopic experiments in separate sessions (36, 37)] in which ODC (Fig. 1*b*) and orientation preference (Fig. 1*c*) were examined. In this region of V1, ODCs are expected to be approximately perpendicular to the calcarine fissure, as shown in Fig. 1*b*. Orientation preference is illustrated as an overlapping and interdependent organization over the same region in Fig. 1*c*; the color scale in this figure corresponds to the calculated phase at the stimulus frequency, which denotes the preferred stimulus orientation of a given voxel. Fig. 2 *a* and *c* illustrate an expanded region of the maps in Fig. 1 *b* and *c*, respectively, along with data from a second subject (Fig. 2 *b* and *d*). ODC borders are marked with solid black lines on both maps. Black and white circles on the orientation maps represent areas where multiple orientation preferences converge, i.e., the so called pinwheel centers. For visualization purposes only, the functional maps shown in Figs. 1 and 2 were spatially filtered with a Gaussian filter. All of the same features are visible in the unfiltered map (supporting information (SI) Fig. S1). All data analyses were preformed on the raw and unfiltered data.

The following spatial characteristics and relationships were found in the orientation preference maps and are illustrated in Fig. 3: (*i*) orientation preference is organized mostly radially, around a point of singularity in a pinwheel like fashion; (*ii*) pinwheels were found to rotate clockwise (CW) (white) and counterclockwise (CCW) (black) (see also Movies 1 and 2); and (*iii*) iso-orientation lines (linear zones), regions where orienta-

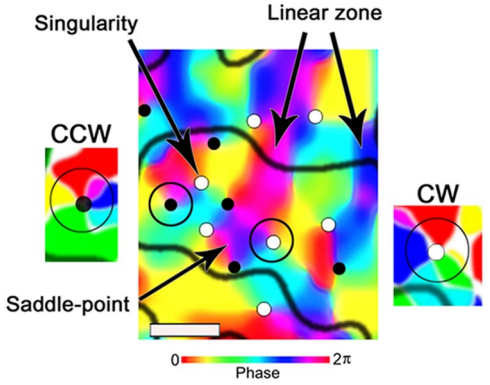

Fig. 3. Spatial features of fMRI maps of orientation preference in human visual cortex. Orientation preference was determined by the temporal phase of fMRI signal changes at the stimulus frequency. The solid black lines indicate the ODC borders. The black or white circles represent singularity points or the centers of the observed radially arranged orientation preference. This radial arrangement can be either CW (white) or CCW (black). Linear zones are regions where the orientation preference changes linearly and tends to extend orthogonally across ODC borders. (Scale bar: 0.5 mm.)

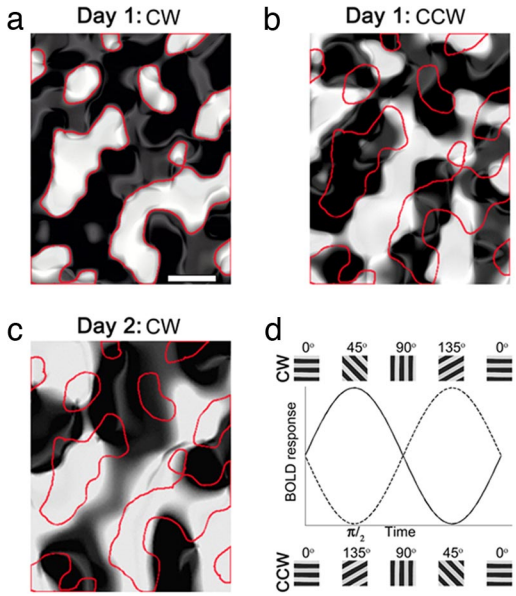

Fig. 4. Reproducibility of orientation preference maps. To test the reproducibility of the phase maps, the displayed orientations were presented through a CW (*a*) or CCW (*b*) rotation while an identical phase-encoding analysis was preformed. At a time point corresponding to a quarter of the cycle, voxels seeing a 45° stimulus during a CW rotation will see a 135° stimulus during a CCW rotation, as schematically illustrated in *d*. Thus, the CW and CCW phase maps should reflect a 180° shift (i.e., complementary maps). For qualitative demonstration, the CW and CCW phase maps (from subject 2) were binned into a 90° bandwidth (*a* and *b*, respectively); bright regions in the CW map were outlined (red) and superimposed on the CCW map. Bright regions in the CW map largely overlap with regions of dark colors in the CCW maps (*b*). Furthermore, good reproducibility is seen with maps acquired on different days (*c*). (Scale bar: 0.5 mm.)

tion preferences change slowly, tend to prefer to cross ODC borders closer to perpendicular orientations rather than parallel. Animal findings have also reported similar tendencies (30, 31). The number of pinwheel centers per spatial area (pinwheel density) was 2.24/mm^2 (eccentricity, 5°), with an average column width (defined as ±15° around 0°, 45°, 90°, or 135° orientations) of 0.77 ± 0.13 mm and a spacing of 1.43 ± 0.12 mm for subject 1, and 1.6/mm^2 (eccentricity, 8°) with an average column width of 0.86 ± 0.13 mm and a spacing of 1.84 ± 0.15 mm in subject 2. The spatial characteristics were further quantified by using the phase dependent magnitude of the Fourier response (32) (see *Methods* and Fig. S2). Differences in the pinwheel densities were observed in conjunction with subtle differences in ODC widths (1.17 ± 0.08 mm and 1.00 ± 0.13 mm for subject 1 and 2, respectively). The discrepancy in columns sizes and pinwheel density likely reflect intrinsic variance between individuals, as is often seen in animal studies (32, 38). Subtle differences in eccentricity and/or inaccurate assignments of pinwheel centers might also contribute to the differences in pinwheel density (39). Assigning a "pinwheel" center (which is by definition a "point" in space) has limited accuracy because of the limited image resolution (40). Even in optical imaging, where the image resolution is much higher, the precise localization of pinwheel centers is limited. Overall, the spatial characteristics of the human fMRI maps were found to be highly consistent with animal models.

Reproducibility and Reliability of the Maps. To test the reproducibility of the phase maps, several approaches were explored. Initially, within a session, the data were separated by odd and even scans and the respective phase maps were compared on a pixel-by-pixel basis [$R = 0.62$ and $R = 0.66$ for subjects 1 and 2, respectively (see Fig. S3 *a* and *b*)]. In an additional experiment, to further establish the repeatability of the observed orientation specific responses, we alternated the stimulus between a CW and a CCW sweep through the different orientations (see Fig. 4*d*) and checked reproducibility, accounting for the reversal of the stimulus presentation ($R = 0.40$) (Fig. S3*c*). This reproducibility is expected to be worse because of ambiguities introduced by the hemodynamic delay.

Grouping the voxels in a 90° bandwidth results in two complementary phase maps (Fig. 4*a*). Reproducibility of such binary maps within a session and between days is illustrated in Fig. 4 *a*–*c*. When such maps are obtained with the stimulus traversing CW vs. CCW (Fig. 4*d*), these binary maps are expected to largely, but not completely, reverse (Fig. 4 *a* vs. *b*). The reversal is not expected to be complete because of the hemodynamic delay. When the stimulus traverses CW, the hemodynamic delay results in a small shift in the observed orientation preference. Because the hemodynamic delay is ≈6 s and one cycle was 60 s, this shift is ≈10% of the orientations sampled (≈18°). When the stimulus rotates CCW, the shift in the depicted orientation preference is in the opposite direction (41). Despite this, the comparisons in Fig. 4 *a* and *b* show large areas of reproducibility.

The reversal of the stimulus traversal (CW vs. CCW) should also result in the reversal of pinwheel directions. In other words, pinwheels, where the orientation preferences are arranged either in the same or opposite rotational direction as the traversal of the stimulus, must reverse when the stimulus traversal direction is reversed. This is illustrated in Movie 3. If the pinwheel patterns are simply artifacts generated from noise, this organized reversal of direction cannot take place.

As a further test of the reliability of the observed spatial patterns, we used the Fourier magnitude analysis (see *Methods* and Fig. S2), which we previously used for spatial characterization of orientation preferences. However, instead of quantifying the spatial profiles of voxels with similar fMRI phases we used random spatial distributions of the orientation-specific phases. This analysis, unlike when the correct spatial information of the calculated phases is used, resulted in a lack of any spatial coherence in the Fourier magnitude as one traveled away from a given column (see Fig. S2). Finally, to demonstrate the relative strength of the response at the stimulus frequency, we plotted the fast Fourier transform (FFT) of the fMRI time course in the gray

matter region of interest (ROI) and compared it with the FFT of temporally scrambled images from the same ROI. The Fourier spectrum distribution of the fMRI time course demonstrated a peak at the stimulus frequency. There are other peaks that can be ascribed to coherent fluctuations in the fMRI time series arising from low-frequency oscillations, cardiac cycle, respiration, and consequent harmonics or folding effects when multiple sources with different frequencies affect the time course. Coherent signal modulations, including the major peak appearing at the stimulus frequency, are eliminated in the temporally shuffled images, demonstrating that their appearance is not attributable to random noise (see Fig. S4).

fMRI sensitivity is paramount to resolving high-resolution functional patterns, as is done in this work. Here, each study comprised of eight to 10 scans (≈7 min per scan) with the subject in the scanner for 2–2.5 h. Generating the functional maps can be performed, however, with much less data averaging, depending on how still the subject remains throughout the scan. For example, in subject 2, we generated two such high-resolution maps (i.e., CW and CCW scans) from the data acquired during one session. Thus, temporal stability, and not fMRI sensitivity, is the limitation in these acquisitions.

Preferred Orientations. A standing debate exists on whether there is a cortical preference (and/or global over-representation) to specific orientation(s). Previous psychophysical and behavioral studies in humans and animals have suggested or predicted either no spatial bias (7, 27, 42–46) or preferences toward both orthogonal orientations (0° and 90°). In the present data, when voxels were binned with a 30° bandwidth around 0°, 45°, 90°, and 135° orientations, a statistically significant ($P_{\text{subject1}} < 0.03$, $P_{\text{subject2}} < 0.07$; see Fig. 5) over-representation (i.e., more voxels preferring) of orientations around 90° (vertical orientation with the grid moving horizontally) was observed in both subjects. The error bars in Fig. 5*a* represent errors between scans within the same subject, and the asterisks represent the significance of the difference between the number of voxels at a given orientation vs. the number of voxels at 90°. To assess whether this over-representation of 90° represented a larger number or larger width of 90° columns, we investigated the spatial autocorrelation of the Fourier magnitude distribution of voxels with similar phases (see Fig. S2). This analysis revealed that column widths or spacing were not statistically different for the 4 phase bins; however, there was a higher regularity or density of columns representing vertical orientations in both subjects. This finding resembles the oblique effect (46–48), which has been demonstrated in the literature through imaging and psychophysical data. The oblique effect refers to greater behavioral sensitivity and larger BOLD changes to both vertical and horizontal orientations compared to oblique (45° and 135°). However, this effect was observed when spanning the entire visual field (all of V1) (46) as opposed to our restricted region. Such significant differences in the amplitude of the BOLD responses could also explain our bias, such that detection is affected in the phase analysis. Such amplitude differences, however, were not observed in our data.

Orientation Tuning Curves. Under our experimental conditions, the functional contrast, i.e., signal change for active vs. nonactive columns, was found to be 67.5 ± 8% and 41 ± 5% for adjacent and complementary columns, respectively (Fig. 5*b*). The ratio of signal changes (nonactive/active) in voxels of a certain orientation preference when experiencing the orthogonal orientation (e.g., 0 vs. 90 or 45 vs. 135°) was ≈0.4, consistent with what was observed in the cat by using cerebral blood flow (CBF)-based fMRI (23). Although no statistical difference in tuning bandwidth was observed between columns, there was a small tendency for orthogonal orientations to better resolve oblique orientations ($r = 0.4$), than the reverse ($r = 0.1$). Interestingly, although there is a tendency of more cortical area being devoted to orientations around 90°, the average increase in fMRI contrast in an "active" column was relatively similar (BOLD change: 0.94 ± 0.22%, subject 1; 1.45 ± 0.27%, subject 2) across all orientations.

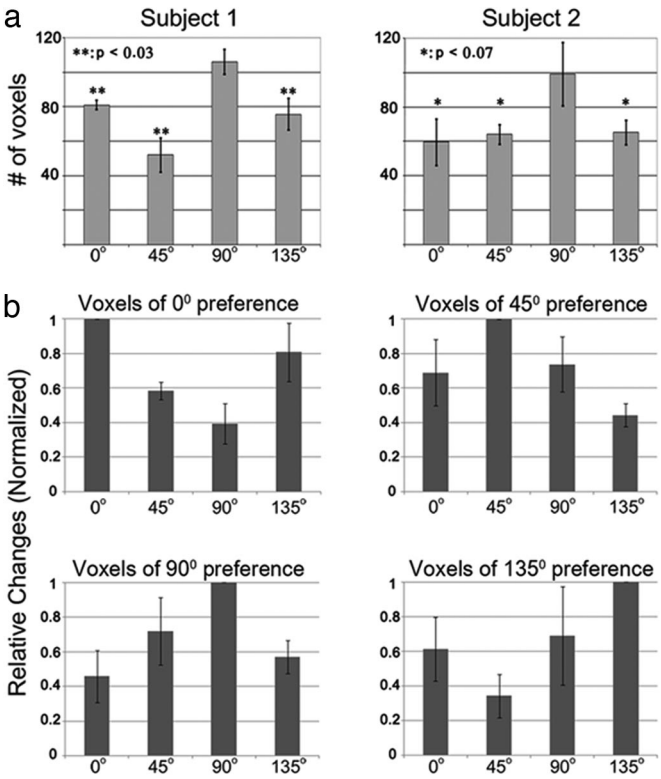

Fig. 5. Quantification of preferred orientation. Column groups in this analysis are defined as those voxels with preferred orientations within ±15 around 0°, 45°, 90°, or 135° orientations. (*a*) Histograms of the number of voxels within each preferred orientation group for each subject. For both subjects, a statistically significant ($P_{\text{subject1}} < 0.03$, $P_{\text{subject2}} < 0.07$) larger number of voxels were tuned to 90° orientations. (*b*) Normalized fMRI signal amplitude changes for each group of orientations, averaged over both subjects. The error bars in *a* represent errors between scans within the same subject, and the asterisks represent the significance of the difference between the number of voxels at a given orientation vs. the number of voxels at 90°.

Imaging Resolution and the BOLD Point Spread Function. We recently reported that when avoiding large vessels, the point spread function (PSF) (Gaussian, full-width half-maximum) of GE BOLD signals at 7 T has an upper limit of 2 mm (49), consistent with a GE-BOLD PSF of 1.6 mm measured in the cat[§]. When the same approach was used, measurements in the cat yielded a PSF of ≈0.7 mm for both SE-BOLD and CBF-based fMRI[†], in agreement with the ability of CBF-based fMRI to yield single-condition orientation maps in the cat (23). Thus, the PSF of the SE-BOLD response should be sufficient to image orientation preference. However, even with GE-BOLD fMRI, it would be feasible to image regular and repeated structures, such as ODCs and orientation preference, provided that large vein areas and discontinuities encountered at boundaries are avoided. This is frequently unappreciated and consequently leads to confusing

[§]Park J, Ronen I, Kim DS, Ugurbil K, Spatial specificity of high resolution GE BOLD and Spin Echo (SE) BOLD fMRI in the cat visual cortex at 9.4 tesla. 13th Scientific Meeting of the International Society for Magnetic Resonance in Medicine, May 7–13, 2005, Miami Beach, FL, abstr 31.

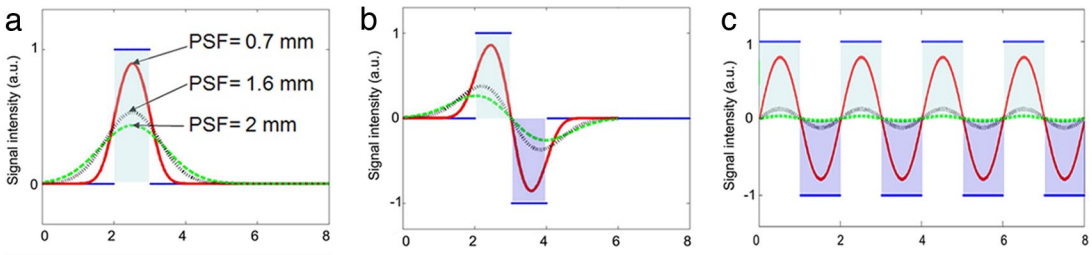

Fig. 6. Effect of the PSF on column mapping. *a* illustrates the intensity distribution that would be measured from a 1D response to a single stimulus that elicits a signal intensity increase of 1 between 2 and 3 mm and 0 everywhere else (blue line) when sampled with a function with a Gaussian PSF (full-width half-maxima) of 0.7, 1.6, and 2 mm. The response is equivalent to what would be seen in ''single-condition'' mapping of a single-element ''column''. *b* shows the plots of the case when there are two such responses between 2 and 3 mm and between 3 and 4 mm for two different stimuli and when these responses are mapped as a difference (i.e., as in differential imaging). *c* shows the results when there are repeated alternating responses to the two different stimuli and when the response is imaged as a difference for the three different PSFs. In this case, the alternating columnar structure extended beyond 0 (in the negative direction) and 8 mm in the positive direction but only the 0- to 8-mm region is illustrated to avoid the edge effects.

arguments about the feasibility of ''columnar'' imaging by fMRI with the different techniques. In imaging of periodic structures, the PSF of the imaging modality affects mainly the CNR, i.e., the relative signal amplitude of the active column relative to its complementary column, and not the ability to accurately define the spatial structure of the different columns. Of course, a low CNR ultimately affects the accuracy of the maps because the boundaries or even the existence of the columns cannot be accurately detected because of the noise. However, if CNR is high enough, then even a method with a larger PSF than the structure to be imaged can yield a map of the structure provided that it is periodic and the PSF is spatially uniform over the area imaged. This concept is illustrated using simulations in Fig. 6 with a 1D structure (2 mm/cycle), resembling human ODCs. Unlike the case of imaging just one column in a single-condition paradigm (Fig. 6*a*), the differential image of the repeated and alternating complementary columnar structure cancels the inaccuracy introduced by the PSF so as to define the boundaries of the structures accurately, albeit with different contrast (Fig. 6 *b* and *c*). The same would be true for multiple, regularly organized representations with similar response properties as in orientation preference mapping. Another advantage of using a technique with a small PSF occurs when the PSF and/or magnitude of the responses is not spatially uniform but has local variance. In fMRI, this is the case because of the presence of large veins distributed sparsely and irregularly, which yield large false ''functional'' responses especially in GE-BOLD (2). In this case, whereas cancellations in differential maps will yield columnar maps in some regions, in others, this cancellation will not be perfect, leading to obscuration of the underlying structure. This has been observed in ODC mapping with GE-BOLD (21). In SE-BOLD at high fields or CBF-based fMRI, this problem is minimized or even eliminated because large vessel contributions are substantially reduced.

Nevertheless, structures with 1-mm dimensions can be mapped in areas void of large vessels, as demonstrated previously in humans (19, 21) and animals (50). In animal models, this is particularly feasible because the geometry of the brain permits imaging in a slice that does not contain surface vasculature (50). Therefore, our data are consistent with the increasing understanding of resolution limits of fMRI and the growing body of animal data that demonstrate the feasibility of columnar mapping with fMRI.

Conclusions

The findings of this study are as follows. First, the data demonstrate directly the existence of orientation preference in human V1 and that the orientation preferences are organized in a striking resemblance to those found in the monkey. Second, the data establish that there is a bias toward processing orientations around 90° (vertical) but not around horizontal. Third, similar fMRI signal changes were found across all orientations. Finally, the impact of neuroimaging on neuroscience research is undisputed; the data and methods presented here specifically demonstrate the feasibility of using fMRI to conduct explorations of previously unmapped, and potentially unknown, columnar systems in the human brain. With the proliferation of high-field MRI systems and constant enhancement of fMRI techniques, an increasing number of studies exploring submillimeter functional structures in humans are anticipated.

Methods

Two healthy men aged 19 and 26 years participated in this study after providing informed consent to the experimental protocol. The human subjects protocol was approved by the institutional review board at the University of Minnesota.

fMRI was conducted on a 7 T whole-body system with a 90-cm bore, driven by a Varian INOVA or a Siemens console. A half-volume radio frequency coil was used for transmission, and a small (6-cm) quadrature coil was used for reception[¶]. For T_2 weighted BOLD imaging, four segments were used with a reduced field of view (3.0×12.8 cm^2) and a 60×256 matrix. The image reception time/echo time was 6 s/55 ms, and the total readout time was 24.0 ms (1.6 ms per line). The nominal in plane spatial resolution was 0.5×0.5 mm^2; however, the data were zero filled and reconstructed to yield images with in plane voxel sizes of 0.25 mm. A 3-mm slice along a flat, minimally curved gray matter area, as posterior as possible through one bank of the calcarine fissure, was selected (19, 21).

To minimize motion, each of the subjects used a bite bar that matched the dental impressions of the subject by using hydroplastic material (Tak Systems). Off-line head motion detection and correction, which caused translation and rotation of the image within the imaged plane, was used (51). The data from scans in which significant motion (mean absolute deviation from the mean position >250 μm) was detected relative to the rest of the data were discarded from the analysis. The average motion parameters for the scans that were used in the averaging were as follows: translation, 0.14 mm $\pm$ 0.04 mm; rotation, 0.38° $\pm$ 0.15° (mean $\pm$ SD of absolute deviation for both parameters). Functional maps from the different days and the different paradigms (ODC and OC) were registered to the same anatomical location.

Visual stimuli were delivered by fiber optics (Silent Vision, Avotec, Inc.), providing visual fields of $23° \times 30°$ either monocularly or binocularly. Subjects were instructed to fixate on a fixation spot throughout the functional scan. Statistical maps and quantitative analysis were done in Stimulate (52) and PV-WAVE (Visual Numerics), and with routines in MATLAB (MathWorks). A voxel-wise *t* test analysis was applied to test whether the BOLD response was higher during epochs of left or right eye stimulation. For orientation, a continuous display of orientations was presented to the subject and the phase of the stimulus correlated fMRI response at the presentation frequency was

[¶]Adriany G, *et al.*, A half-volume transmit/receive coil combination for 7 tesla applications. 9th Scientific Meeting of the International Society for Magnetic Resonance in Medicine, April 21–27, 2001, Glasgow, Scotland, abstr 1097.

NEUROSCIENCE

used to distinguish voxels with different orientation preferences (41), as is routinely done with standard retinotopic mapping. The parameters of the orientation stimuli were as follows: spatial frequency, two cycles per degree; drift velocity, four cycles per second; drift reversal every second, one cycle (180° of orientation) per minute and six cycles per scan. To facilitate visualization of the spatial patterns in the functional maps, a Gaussian filter was applied (see Fig. S1). All quantification and analysis, however, were done by using the raw data. To quantify the spatial characteristics (i.e., column width, spacing, and density) of orientation preference (using four bins; ±15° around 0°, 45°, 90°, and 135°), we took the magnitude of the Fourier transform of the fMRI time course at the stimulus frequency (Fig. S2) to obtain a measure of the response strength and how it varies in space for each of the four bins of Fourier phases. We then computed the spatial autocorrelation of the response strengths (Fourier magnitude) for each phase group or set of voxels that preferred similar orientations (32). The resulting 2D spatial distribution was collapsed (averaged) to generate a projected 1D profile that represented the average spatial profile of orientation columns. The same analysis was done to test the noise in the data by randomizing the spatial locations of each of the calculated phases (Fig. S2).

ACKNOWLEDGMENTS. We thank Dr. Cheryl Olman for the retinotopic data; Drs. G. M. Ghose, R. A. Galuske, and J. L. Gardner for helpful discussions; and Drs. G. Adriany and P. Anderson for hardware support. This work was supported, in part, by National Institutes of Health Grants P41 RR08079, R01 MH070800, R01 EB000331, and P30 NS057091; the W. M. Keck Foundation; and the Mind Research Network for Neurodiagnostic Discovery (MRN). The 7 T magnet acquisition was funded, in part, by National Science Foundation Grant DBI-9907842 and National Institutes of Health Grant S10 RR1395.

1. Vaughan JT, *et al.* (2001) 7T vs. 4T: RF power, homogeneity, and signal-to-noise comparison in head images. *Magn Reson Med* 46:24–30.
2. Ugurbil K, *et al.* (2003) Ultrahigh field magnetic resonance imaging and spectroscopy. *Magn Reson Imaging* 21:1263–1281.
3. Lorente de No' R (1938) Architectonics and structure of the cerebral cortex. *Physiology of the Nervous System*, ed Fulton JF (Oxford Univ Press, New York), pp 291–330.
4. Mountcastle VB (1957) Modality and topographic properties of single neurons of cat's somatic sensory cortex. *J Neurophysiol* 20:408–434.
5. Woolsey TA, Van der Loos H (1970) The structural organization of layer IV in the somatosensory region (SI) of mouse cerebral cortex. The description of a cortical field composed of discrete cytoarchitectonic units. *Brain Res* 17:205–242.
6. Hubel DH, Wiesel TN (1959) Receptive fields of single neurones in the cat's striate cortex. *J Physiol* 148:574–591.
7. Hubel DH, Wiesel TN (1962) Receptive fields, binocular interaction and functional architecture in the cat's visual cortex. *J Physiol* 160:106–154.
8. Hubel DH, Wiesel TN (1968) Receptive fields and functional architecture of monkey striate cortex. *J Physiol* 195:215–243.
9. Blasdel GG, Salama G (1986) Voltage-sensitive dyes reveal a modular organization in monkey striate cortex. *Nature* 321:579–585.
10. Bonhoeffer T, Grinvald A (1991) Iso-orientation domains in cat visual cortex are arranged in pinwheel-like patterns. *Nature* 353:429–431.
11. Hubel DH, Wiesel TN (1963) Shape and arrangement of columns in cat's striate cortex. *J Physiol* 165:559–568.
12. Hubel DH, Wiesel TN (1977) Ferrier lecture. Functional architecture of macaque monkey visual cortex. *Proc R Soc London Ser B* 198:1–59.
13. Shmuel A, Grinvald A (1996) Functional organization for direction of motion and its relationship to orientation maps in cat area 18. *J Neurosci* 16:6945–6964.
14. Shoham D, Hubener M, Schulze S, Grinvald A, Bonhoeffer T (1997) Spatio-temporal frequency domains and their relation to cytochrome oxidase staining in cat visual cortex. *Nature* 385:529–533.
15. Weliky M, Bosking WH, Fitzpatrick D (1996) A systematic map of direction preference in primary visual cortex. *Nature* 379:725–728.
16. Horton J, Hedley-Whyte ET (1984) Mapping of cytochrome oxidase patches and ocular dominance columns in human visual cortex. *Philos Trans R Soc London Ser B* 304:255–272.
17. Menon R, Ogawa S, Strupp JP, Ugurbil K (1997) Ocular dominance in human V1 demonstrated by functional magnetic resonance imaging. *J Neurophysiol* 77:2780–2787.
18. Goodyear BG, Menon RS (2001) Brief visual stimulation allows mapping of ocular dominance in visual cortex by using fMRI. *Hum Brain Mapp* 14:210–217.
19. Cheng K, Waggoner RA, Tanaka K (2001) Human ocular dominance columns as revealed by high-field functional magnetic resonance imaging. *Neuron* 32:359–374.
20. Dechent P, Frahm J (2000) Direct mapping of ocular dominance columns in human primary visual cortex. *Neuroreport* 11:3247–3249.
21. Yacoub E, Shmuel A, Logothetis N, Ugurbil K (2007) Robust detection of ocular dominance columns in humans using Hahn Spin Echo BOLD functional MRI at 7 tesla. *NeuroImage* 37:1161–1177.
22. Sun P, *et al.* (2007) A temporal frequency-dependent functional architecture in human V1 revealed by high-resolution fMRI. *Nat Neurosci* 10:1404–1406.
23. Duong TQ, Kim DS, Ugurbil K, Kim SG (2001) Localized cerebral blood flow response at submillimeter columnar resolution. *Proc Natl Acad Sci USA* 98:10904–10909.
24. Harel N, Lin J, Moeller S, Ugurbil K, Yacoub E (2006) Combined imaging-histological study of cortical laminar specificity of fMRI signals. *NeuroImage* 29:879–887.
25. Moon CH, Fukuda M, Park SH, Kim SG (2007) Neural interpretation of blood oxygenation level-dependent fMRI maps at submillimeter columnar resolution. *J Neurosci* 27:6892–6902.
26. Blasdel GG (1992) Differential imaging of ocular dominance and orientation selectivity in monkey striate cortex. *J Neurosci* 12:3115–3138.
27. Hubel DH, Wiesel TN (1974) Sequence regularity and geometry of orientation columns in the monkey striate cortex. *J Comp Neurol* 158:267–293.
28. Haynes JD, Rees G (2005) Predicting the orientation of invisible stimuli from activity in human primary visual cortex. *Nat Neurosci* 8:686–691.
29. Kamitani Y, Tong F (2005) Decoding the visual and subjective contents of the human brain. *Nat Neurosci* 8:679–685.
30. Bartfeld E, Grinvald A (1992) Relationships between orientation-preference pinwheels, cytochrome oxidase blobs, and ocular-dominance columns in primate striate cortex. *Proc Natl Acad Sci* 89:11905–11909.
31. Hubener M, Shoham D, Grinvald A, Bonhoeffer T (1997) Spatial relationships among three columnar systems in cat area 17. *J Neurosci* 17:9270–9284.
32. Obermayer K, Blasdel GG (1993) Geometry of orientation and ocular dominance columns in monkey striate cortex. *J Neurosci* 13:4114–4129.
33. Tootell RB, Hamilton SL, Silverman MS, Switkes E (1988) Functional anatomy of macaque striate cortex. I. Ocular dominance, binocular interactions, and baseline conditions. *J Neurosci* 8:1500–1530.
34. Ts'o DY, Frostig RD, Lieke EE, Grinvald A (1990) Functional organization of primate visual cortex revealed by high resolution optical imaging. *Science* 249:417–420.
35. Horton J, Dagi L, McCrane E, de Monasterio F (1990) Arrangement of ocular dominance columns in human visual cortex. *Arch Ophthalmol* 108:1025–1031.
36. Engel SA, Glover GH, Wandell BA (1997) Retinotopic organization in human visual cortex and the spatial precision of functional MRI. *Cereb Cortex* 7:181–192.
37. Wandell BA, Dumoulin SO, Brewer AA (2007) Visual field maps in human cortex. *Neuron* 56:366–384.
38. Engelmann R, Crook JM, Lowel S (2002) Optical imaging of orientation and ocular dominance maps in area 17 of cats with convergent strabismus. *Vis Neurosci* 19:39–49.
39. Vanduffel W, Tootell RB, Schoups A, Orban GA (2002) The organization of orientation selectivity throughout macaque visual cortex. *Cereb Cortex* 12:647–662.
40. Polimeni JR, Granquist-Fraser D, Wood RJ, Schwartz EL (2005) Physical limits to spatial resolution of optical recording: clarifying the spatial structure of cortical hypercolumns. *Proc Natl Acad Sci USA* 102:4158–4163.
41. Kalatsky VA, Stryker MP (2003) New paradigm for optical imaging: Temporally encoded maps of intrinsic signal. *Neuron* 38:529–545.
42. Li B, Peterson MR, Freeman RD (2003) Oblique effect: A neural basis in the visual cortex. *J Neurophysiol* 90:204–217.
43. Bonhoeffer T, Grinvald A (1993) The layout of iso-orientation domains in area 18 of cat visual cortex: Optical imaging reveals a pinwheel-like organization. *J Neurosci* 13:4157–4180.
44. Chapman B, Bonhoeffer T (1998) Overrepresentation of horizontal and vertical orientation preferences in developing ferret area 17. *Proc Natl Acad Sci USA* 95:2609–2614.
45. Wang G, Ding S, Yunokuchi K (2003) Difference in the representation of cardinal and oblique contours in cat visual cortex. *Neurosci Lett* 338:77–81.
46. Furmanski CS, Engel SA (2000) An oblique effect in human primary visual cortex. *Nat Neurosci* 3:535–536.
47. Mansfield RJ (1974) Neural basis of orientation perception in primate vision. *Science* 186:1133–1135.
48. Orban GA, Vandenbussche E, Vogels R (1984) Human orientation discrimination tested with long stimuli. *Vision Res* 24:121–128.
49. Shmuel A, Yacoub E, Chaimow D, Logothetis NK, Ugurbil K (2007) Spatio-temporal point-spread function of fMRI signal in human gray matter at 7 tesla. *NeuroImage* 35:539–552.
50. Bolan PJ, Yacoub E, Garwood M, Ugurbil K, Harel N (2006) In vivo micro-MRI of intracortical neurovasculature. *NeuroImage* 32:62–69.
51. Woods RP, Cherry SR, Mazziotta JC (1992) Rapid automated algorithm for aligning and reslicing PET images. *J Comput Assist Tomogr* 16:620–633.
52. Strupp JP (1996) Stimulate: A GUI based fMRI analysis software package. *NeuroImage* 3:S607.